



Cite this: *RSC Adv.*, 2023, **13**, 18129

## Adsorption and sensing mechanisms of Ni-doped PtTe<sub>2</sub> monolayer upon NO<sub>2</sub> and O<sub>3</sub> in air-insulated switchgears†

Zhuoli Xu  \*

Under partial discharge, air would be converted into O<sub>3</sub> and NO<sub>2</sub> in air-insulated switchgears, therefore, the detection of such two gases can be used to evaluate the operation status of such electrical equipment. In this study, first-principles simulations are implemented to investigate the Ni-doping behavior on the pristine PtTe<sub>2</sub> monolayer, and the adsorption and sensing performances of the Ni-doped PtTe<sub>2</sub> (Ni–PtTe<sub>2</sub>) monolayer upon O<sub>3</sub> and NO<sub>2</sub> in air-insulated switchgears. The formation energy ( $E_{\text{form}}$ ) of Ni-doping on the PtTe<sub>2</sub> surface was calculated to be  $-0.55$  eV, which indicates the exothermicity and spontaneity of the Ni-doping process. Strong interactions occurred in the O<sub>3</sub> and NO<sub>2</sub> systems given the significant adsorption energy ( $E_{\text{ad}}$ ) of  $-2.44$  and  $-1.93$  eV, respectively. Using the band structure and frontier molecular orbital analysis, the sensing response of the Ni–PtTe<sub>2</sub> monolayer upon such two gas species is quite close and large enough for gas detections. Combined with the extremely long recovery time for gas desorption, it is presumed that the Ni–PtTe<sub>2</sub> monolayer is a promising one-shot gas sensor for O<sub>3</sub> and NO<sub>2</sub> detection with a strong sensing response. This study aims at proposing a novel and promising gas sensing material for the detection of the typical fault gases in air-insulated switchgears, so as to ensure their good operation in the whole power system.

Received 7th May 2023  
 Accepted 1st June 2023

DOI: 10.1039/d3ra03030j  
[rsc.li/rsc-advances](http://rsc.li/rsc-advances)

### 1. Introduction

Air-insulated switchgear is an important type of high-voltage electrical equipment, mainly applied to protect and control the equipment in the power system, such as transformers, generators, capacitors, and cables, to ensure the safety and normal operation of the whole power system.<sup>1</sup> In air-insulated switchgears, the air is used as the insulation medium to prevent partial discharge in the equipment, therefore, they are tremendously applied in medium and low-voltage power equipment owing to their unique merits of low cost and good performance.<sup>2</sup> However, after a long time running, some inevitable insulation defects, including partial discharge and electric corona, would occur in such kind of equipment, decomposing the air into two toxic gas species, including NO<sub>2</sub> and O<sub>3</sub>,<sup>2,3</sup> wherein the partial overheat can facilitate such process dramatically. With the increasing percentage of unserviceable gases, the insulation performance of air, in which the N<sub>2</sub> as the dominant species undertakes the insulation mission, would be weakened.<sup>4</sup> This would pose a great threat to the safe operation of air-insulated switchgears and the whole power

grid.<sup>5</sup> From this regard, the detection of the above-mentioned typical gases has been proposed and proved as a workable and effective approach to estimate the severity degree of the inner insulation defects in the air-insulated switchgears and their working conditions,<sup>6–8</sup> which has become the hotspot in the gas sensing field.<sup>9,10</sup>

Regarding gas sensing techniques, the nano-sensing method in recent years has been promoted largely owing to the dramatic developments of materials science and the remarkable advantages of such a method with good electric response and easy preparation.<sup>11,12</sup> In comparison to traditional sensing materials, such as metal oxides and carbon nanotubes,<sup>13,14</sup> two-dimensional (2D) nanomaterials can perform better adsorption performance upon gas species owing to their larger surface areas and stronger electron mobility.<sup>15</sup> Therefore, the electrical response of the 2D nanomaterial-based gas sensor is promoted largely, giving rise to their strong potential for gas sensing explorations.<sup>16–19</sup> Very recently, the transition metal dichalcogenides, namely TMDs, are paid remarkable attention to gas sensing and nano-electronic devices.<sup>20–23</sup> Especially, noble TMDs, such as PtS<sub>2</sub> and PtSe<sub>2</sub>, are successfully synthesized and theoretically verified with different electronic properties in comparison to MoS<sub>2</sub> and MoSe<sub>2</sub>.<sup>24,25</sup> For example, PtS<sub>2</sub> and PtSe<sub>2</sub> monolayers, especially through the transition (TM) doping process, are thoroughly proven with great sensing properties and electrical response upon the gas molecules, with desirable potential for exploration as the nano-electronic devices,<sup>26–29</sup> in

*Huber Engineering Research Center for Safety Monitoring of New Energy and Power Grid Equipment, Huber University of Technology, Wuhan, 430068, China. E-mail: [xzl772010568@163.com](mailto:xzl772010568@163.com)*

† Electronic supplementary information (ESI) available. See DOI: <https://doi.org/10.1039/d3ra03030j>



which the TM dopant plays an effective role to enhance the charge-transfer in the gas interactions, therefore, promoting the sensing response in the gas detections.

On the other hand, the  $\text{PtTe}_2$  monolayer, to the best of our knowledge, is purposed for  $\text{NO}_2$  sensing with ultra-high sensitivity and selectivity.<sup>30</sup> Besides, the Ru-doped  $\text{PtTe}_2$  monolayer has been investigated for the detection of exhaled breath gases so as to explore its potential for the diagnosis of lung cancer.<sup>31</sup> Also, there are several up-to-date reports about its structural and electronic properties,<sup>32–34</sup> as well as the TM-doping performance.<sup>35</sup> In this research, the unique electronic properties and the desirable chemical reactivity are proved, which is beneficial to explore its potential as a gas sensor, especially with the TM atom doped. Considering the remarkable catalytic behavior of the Ni dopant in the gas interactions to enhance the sensing response of the 2D nano-systems,<sup>36–38</sup> we propose Ni-doped  $\text{PtTe}_2$  ( $\text{Ni-PtTe}_2$ ) monolayer in this paper, based on the first-principles calculations, as a novel candidate for  $\text{NO}_2$  and  $\text{O}_3$  detection in the air insulated switchgear. A Ni atom is substituted by a Te atom to model the  $\text{Ni-PtTe}_2$  configuration and to analyze the Ni-doping performance on the physico-chemical properties of the  $\text{PtTe}_2$  monolayer, with a similar method from ref. 39. The findings in this theoretical work can provide detailed guidance to explore  $\text{PtTe}_2$ -based gas sensors for toxic gas detection in electrical engineering, which is also helpful for their further explorations in many other fields.

## 2. Computational details

The spin-unrestricted calculations were used in this work to perform all the first-principles simulations within the  $\text{DMol}^3$  package,<sup>40</sup> by which the Perdew–Burke–Ernzerhof (PBE) function within the generalized gradient approximation (GGA) was determined to deal with the exchange–correlation interaction.<sup>41</sup> The crystal as a whole is geometrically optimized using the BFGS method in the  $\text{DMol}^3$  package. The DFT-D2 corrected dispersion was applied to consider the van der Waals force and long-range interactions.<sup>42</sup> A  $k$ -point mesh of  $10 \times 10 \times 1$  in the Monkhorst–Pack–Brillouin zone was defined for the whole geometric and electronic calculations.<sup>43</sup> Besides, we defined the energy tolerance accuracy, self-consistent loop energy, and the global orbital cut-off radius to be  $10^{-5}$  Ha,  $10^{-6}$  Ha, and  $5.0 \text{ \AA}$ , respectively.

In the current work, we established a  $3 \times 3 \times 1$  supercell for the pristine  $\text{PtTe}_2$  monolayer to conduct the following calculations. Besides, the vacuum region was determined to be  $18 \text{ \AA}$  along the  $z$  direction to prevent probable interactions between the neighboring units.<sup>45</sup> The formation energy ( $E_{\text{form}}$ ) is defined to reflect the required energy to substitute a Te atom with a Ni dopant on the pristine  $\text{PtTe}_2$  surface, and the gas adsorption energy ( $E_{\text{ad}}$ ) is defined to reflect the gas interaction strength on the  $\text{Ni-PtTe}_2$  monolayer, calculated by:<sup>46</sup>

$$E_{\text{form}} = E_{\text{Ni-PtTe}_2} - E_{\text{PtTe}_2} - \mu_{\text{Ni}} + \mu_{\text{X}} \quad (1)$$

$$E_{\text{ad}} = E_{\text{Ni-PtTe}_2/\text{gas}} - E_{\text{Ni-PtTe}_2} - E_{\text{gas}} \quad (2)$$

where  $E_{\text{Ni-PtTe}_2}$  and  $E_{\text{PtTe}_2}$  represent the total energy of the Ni-doped and the pristine  $\text{PtTe}_2$  monolayer, respectively, while the  $\mu_{\text{Ni}}$  and  $\mu_{\text{X}}$  represent the chemical potential of per Ni and replaced Te or Pt atom in their bulk structures, respectively.  $E_{\text{Ni-PtTe}_2/\text{gas}}$  and  $E_{\text{gas}}$  represent the total energies of the gas-adsorbed system and isolated gas molecule, respectively. Moreover, the charged value of the Ni dopant ( $Q_{\text{Ni}}$ ) in its substituting process and that of the gas species ( $Q_{\text{T}}$ ) in the gas adsorption systems were considered by the Mulliken analysis.<sup>47</sup>

## 3. Results and discussion

### 3.1 Ni-doping behavior on the $\text{PtTe}_2$ monolayer

The Ni-doping process on the  $\text{PtTe}_2$  monolayer is plotted in Fig. 1, in which Fig. 1(a) shows the pristine  $\text{PtTe}_2$  monolayer, whereas Fig. 1(b) and (c) show the configurations of  $\text{Ni-PtTe}_2$  monolayer and related charge density difference (CDD). For the pristine  $\text{PtTe}_2$  monolayer, the lattice constant and the Pt–Te bond with geometric optimization were obtained as  $4.03$  and  $2.74 \text{ \AA}$ , respectively, which are consistent with the previously reported values of  $4.02$  and  $2.76 \text{ \AA}$ ,<sup>32</sup> respectively, verifying that the calculations in this work were reliable. When the  $\text{Ni-PtTe}_2$  monolayer is formed by substituting a Te atom with the Ni atom, one can see that the Ni atom is shrunk within the Te atomic layer and the Ni–Pt bond length, measured to be  $2.51 \text{ \AA}$ , is much shorter than that of the Pt–Te bond ( $2.74 \text{ \AA}$ ). This to a large extent is attributed to the much shorter atomic radii of the Ni dopant compared to the Te atom.<sup>48</sup> Besides, the  $E_{\text{form}}$  for Ni-doping on the  $\text{PtTe}_2$  surface by replacing the Te atom was calculated to be  $-0.55 \text{ eV}$ , and by replacing the Pt atom was calculated to be  $1.08 \text{ eV}$ . That is, the substitution of a Te atom by a Ni dopant on the  $\text{PtTe}_2$  monolayer was exothermic while the substitution of a Pt atom by a Ni dopant on the  $\text{PtTe}_2$  monolayer was not energy-favorable. In other words, the Ni-doping process would be more likely to occur by replacing the Te atom on the pristine  $\text{PtTe}_2$  monolayer, and by such means, the synthesis of  $\text{Ni-PtTe}_2$  monolayer was fully procurable and spontaneous at room temperature,<sup>49,50</sup> which is beneficial to reduce the difficulty for its synthesis from the large-scale point of view. Moreover, we performed the DFT +  $U$  method (the  $U$  value was set as  $3 \text{ eV}$ ) to calculate the  $E_{\text{form}}$  for Ni-doping on the pristine  $\text{PtTe}_2$  monolayer by replacing the Te atom, and the  $E_{\text{form}}$  was calculated as  $-0.58 \text{ eV}$ . Such a finding indicates that the DFT +  $U$  method has no big impact on the Ni-doping process.

According to the Mulliken analysis, the Te dopant is positively charged by  $0.229e$  in the pristine  $\text{PtTe}_2$  monolayer, while the Ni dopant at the Te atomic site is positively charged by  $0.211e$  in the  $\text{Ni-PtTe}_2$  system. That is, the Te atom shows stronger electron-donating properties than the Ni dopant when bonding with the Pt atom, which is consistent with their electronegativities, in the order of Pt (2.28) > Te (2.10) > Ni (1.91).<sup>51</sup> From the CDD, the Ni dopant is surrounded by electron depletion while the Ni–Pt bonds are embraced by the electron accumulation, which indicates the electron-releasing property of the Ni dopant when doping on the  $\text{PtTe}_2$  surface as well as the strong binding force of the Ni–Pt bonds. Also, these electron



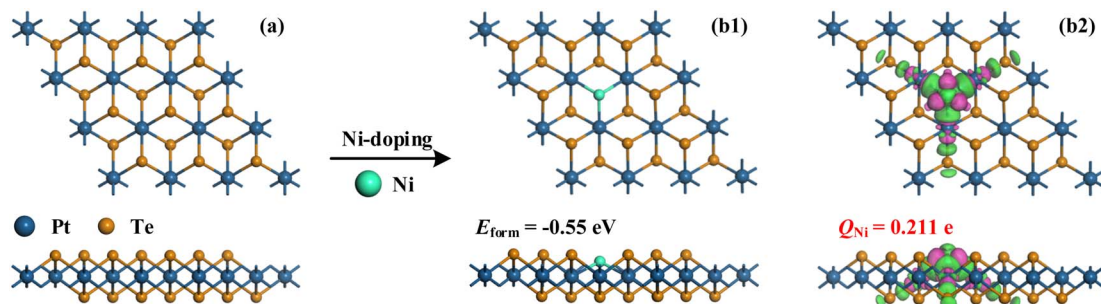


Fig. 1 Ni-doping configuration on the PtTe<sub>2</sub> monolayer. (a) Pristine PtTe<sub>2</sub> monolayer, (b1) and (b2) structure of Ni-PtTe<sub>2</sub> monolayer and related CDD. In CDD, the green area is electron accumulation, while the rosy area is electron depletion, and the isosurface was 0.01 eV Å<sup>-3</sup>.

distributions are in good agreement with the Mulliken population analysis.

Fig. 2 shows the band structure (BS) of the pristine and Ni-doped PtTe<sub>2</sub> monolayer as well as the orbital density of state (DOS) of the atoms in the Ni-Pt bond, in order to deeply comprehend the electronic property of Ni-doping on the PtTe<sub>2</sub> surface. From the BS of the pristine PtTe<sub>2</sub> monolayer, the top valence band and the bottom conduction band are *r* localized on the  $\Gamma$  and  $K$  point, respectively, and the bandgap was obtained as 0.612 eV. These findings are in good accordance with the previous report,<sup>30</sup> which revealed the indirect semiconducting property for the pristine PtTe<sub>2</sub> monolayer with a bandgap of 0.69 eV based on the GGA function, and it is worth noting that such a small difference in bandgap could be ascribed to the different basic set in the diverse calculations. For the Ni-PtTe<sub>2</sub> monolayer, one can see that the top valence band and the bottom conduction band are both localized on the  $K$  point with a bandgap of 0.506 eV. These findings indicate that Ni-doping not only narrows the bandgap, but also modifies the indirect semiconducting property of the pristine PtTe<sub>2</sub> monolayer making it become a direct semiconductor, which might be beneficial for its further exploration in the optical field. Besides, the spin-up is symmetric with the spin-down, which revealed the non-magnetic property of the Ni-PtTe<sub>2</sub> monolayer, namely

Ni-doping has no impact on the magnetic property of the PtTe<sub>2</sub> monolayer. From the atomic DOS, the Ni 3d orbital is highly hybrid with the Pt 5d orbital at -3.3, -2.8, -1.6-0, and 0.4-0.9 eV, which revealed the admirable orbital interaction between the Ni dopant and the Pt atom, verifying the strong binding force of the Ni-Pt bonds.<sup>52</sup>

### 3.2 Gas adsorptions on Ni-PtTe<sub>2</sub> monolayer

O<sub>3</sub> and NO<sub>2</sub> adsorptions on the Ni-PtTe<sub>2</sub> monolayer were performed around the Ni dopant using various configurations with the distance between the gas species and the Ni dopant appropriate 2.5 Å, which is a proper empirical value to initiate surface interactions in the previous report.<sup>53</sup> For O<sub>3</sub> adsorption above the Ni atom, three configurations are considered, namely the molecule-parallel position, two non-bonded O atom-oriented positions, and the middle O atom-oriented position. Also, For NO<sub>2</sub> adsorption above the Ni atom, three configurations can be traced, namely the molecule-parallel position, two O atom-oriented positions, and the N atom-oriented position. With full relaxation, the most stable configuration (MSC) for gas adsorptions in line with related CDD is depicted in Fig. 3.

In the O<sub>3</sub> adsorption system, the O<sub>3</sub> molecule is somewhat vertical to the Ni-PtTe<sub>2</sub> surface and two non-bonded O atoms

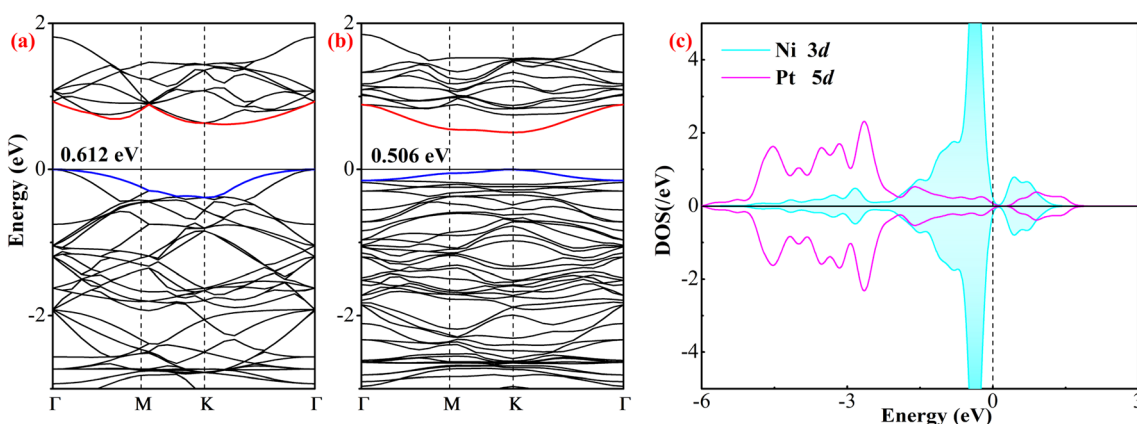


Fig. 2 Electronic property of pristine and Ni-doped PtTe<sub>2</sub> monolayer. (a) and (b) BS of pristine and Ni-doped PtTe<sub>2</sub> monolayer, and (c) orbital DOS of Ni dopant and Pt atom. In BS, the red and blue lines signify the bottom conduction band and top valence band, respectively, and the black values are the bandgaps. In DOS, the Fermi level was set as 0 eV.



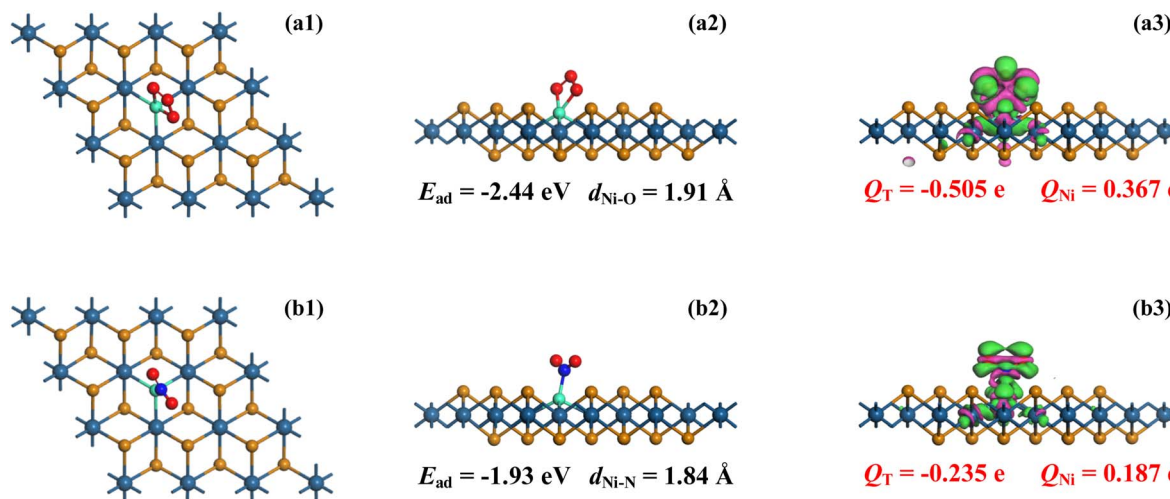


Fig. 3 MSC in the top and side view as well as the CDD of (a1)–(a3)  $O_3$  system and (b1)–(b3)  $NO_2$  system. In CDD, the basic sets are the same as that in Fig. 1.

are captured by the Ni dopant, forming two Ni–O bonds, with lengths of 1.91 and 1.93 Å, respectively. The  $E_{ad}$  for  $O_3$  adsorption on the Ni–PtTe<sub>2</sub> monolayer was calculated to be  $-2.44$  eV, whose absolute value is significantly larger than the critical value of  $0.80$  eV<sup>54</sup> to clarify such interaction as chemisorption. Besides, we should mention that the adsorption performance of the Ni–PtTe<sub>2</sub> monolayer upon  $O_3$  is stronger than that of the Pd-doped GaN nanotube and Rh-doped ZnO monolayer given the more negative  $E_{ad}$  here compared with those of  $-1.548$  eV<sup>2</sup> in the former system and  $-1.35$  eV<sup>55</sup> in the latter system. At the same time, such a value indicates the strong binding force of the Ni–O bonds that gives rise to the remarkable  $E_{ad}$  in this system. From the Mulliken population analysis, the  $O_3$  molecule is negatively charged by  $0.505e$  while the Ni dopant is positively charged by  $0.367e$ . From these results, one can infer that in the  $O_3$  adsorption process, the  $O_3$  molecule accepts  $0.505e$  in total from the Ni–PtTe<sub>2</sub> surface, among which  $0.156e$  is donated by the Ni dopant while  $0.349e$  is donated by the PtTe<sub>2</sub> monolayer. From the CDD, the  $O_3$  molecule is embraced by the electron accumulation as well as the Ni–O bonds, while the Ni dopant is surrounded by the electron depletion. The electron distributions not only verified the Mulliken population analysis, but also proved the strong electron-accepting property of the  $O_3$  molecule in the gas interactions.<sup>56</sup>

For  $NO_2$  adsorption on the Ni–PtTe<sub>2</sub> monolayer, it was seen that the  $NO_2$  molecule, similar to that in the  $O_3$  system, was also vertical to the PtTe<sub>2</sub> surface and the N atom was trapped by the Ni dopant forming a Ni–N bond as measured to be 1.84 Å. The  $E_{ad}$  herein was obtained as  $-1.93$  eV, whose absolute value is smaller than that in the  $O_3$  system. Even though, chemisorption could be identified as well given the judging terms of the critical value (absolute  $E_{ad}$  larger than  $0.8$  eV<sup>57</sup>). Such  $E_{ad}$  is comparable with that in the PdN<sub>3</sub>-doped CNT system in which the  $E_{ad}$  is obtained as  $-1.91$  eV for  $NO_2$  adsorption<sup>58</sup> and is more negative than that in the Rh-doped MoSe<sub>2</sub> monolayer in which the  $E_{ad}$  is obtained as  $-1.88$  eV for  $NO_2$  adsorption.<sup>59</sup> Besides, the bond

length of Ni–N in the  $NO_2$  system is shorter than the Ni–O in the  $O_3$  system by  $0.07$  Å. Considering the larger atomic radii of N compared to O by  $0.08$  Å (N is  $71$  Å and O is  $63$  Å<sup>48</sup>), the stronger interaction in the  $O_3$  system in comparison to the  $NO_2$  system could also be verified, thereby narrowing the Ni–N bond much more than the Ni–O bond. According to the Mulliken population analysis, the  $NO_2$  molecule is charged by  $-0.235e$ , while the Ni dopant is charged by  $0.187e$ . In other words, the  $NO_2$  molecule and the Ni dopant accept  $0.235$  and  $0.024e$ , respectively, from the PtTe<sub>2</sub> monolayer which behaves as an electron donator, relieving  $0.259e$  in total for  $NO_2$  adsorption. From the CDD, there have strong electron accumulations dominantly on the  $NO_2$  molecule, the Ni dopant, and the Ni–N bond, which agrees with the Mulliken population analysis well.

Moreover, we should note that considering the size effect of the Ni–PtTe<sub>2</sub> supercell, we performed the adsorption of  $O_3$  and  $NO_2$  on the  $4 \times 4 \times 1$  Ni–PtTe<sub>2</sub> monolayer. To accomplish this, the pristine and Ni-doped  $4 \times 4 \times 1$  PtTe<sub>2</sub> monolayer should be geometrically optimized as well. The obtained configurations are plotted in Fig. S1.† From Fig. S1† we can find that the  $E_{form}$  for Ni-doping on the pristine  $4 \times 4 \times 1$  PtTe<sub>2</sub> monolayer ( $-0.60$  eV) is somewhat impacted, becoming slightly negative in comparison with that of  $-0.55$  eV in the  $3 \times 3 \times 1$  PtTe<sub>2</sub> monolayer. On the other hand, the adsorption performance of the  $4 \times 4 \times 1$  Ni–PtTe<sub>2</sub> monolayer has changed little compared with the  $3 \times 3 \times 1$  Ni–PtTe<sub>2</sub> monolayer, indicating that the  $3 \times 3 \times 1$  supercell would be large enough and suitable for performing adsorption of  $O_3$  and  $NO_2$ .

### 3.3 Electronic property analysis

All the above analyses reveal the stronger adsorption performance of the Ni–PtTe<sub>2</sub> monolayer upon  $O_3$  compared to  $NO_2$ , therefore, one can assume that the electronic response in the  $O_3$  system might be much larger than that in the  $NO_2$  system. Fig. 4 depicts the BS, frontier molecular orbital (FMO), and atomic DOS of two gas systems. It is worth noting that the FMO is also



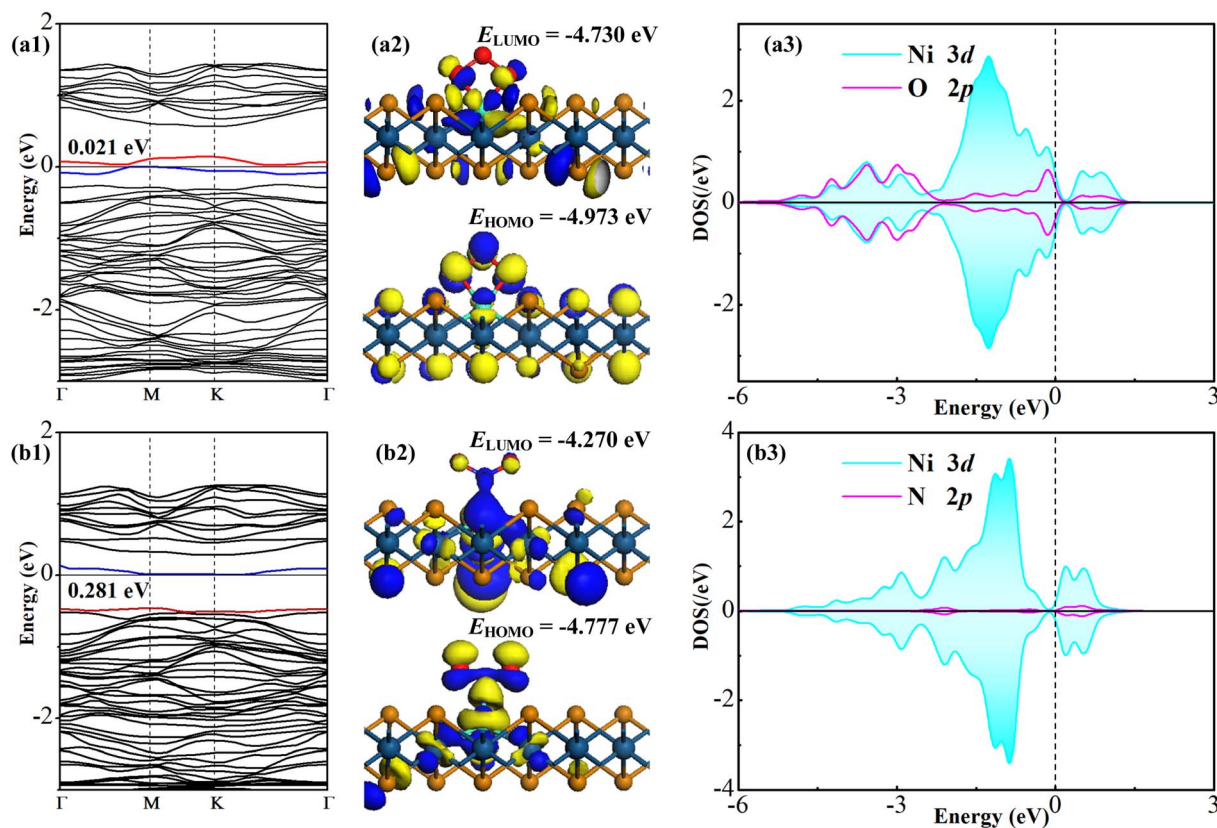


Fig. 4 BS, FMO and atomic DOS of (a1)–(a3)  $\text{O}_3$  system and (b1)–(b3)  $\text{NO}_2$  system.

an important parameter, which includes the highest occupied molecular orbital (HOMO) and lowest unoccupied molecular orbital (LUMO), to reflect the electrical conductivity (resistance) of the system according to the energy gap ( $E_g$ ) between the HOMO and LUMO. The larger  $E_g$  indicates the smaller (larger) electrical conductivity (resistance).<sup>60</sup> Also, we should note that we only plotted the orbital DOS of the outermost electron shell of the bonded atoms in order to directly and effectively reflect the orbital interaction between them. Besides, we plotted the FMO of the pure Ni-PtTe<sub>2</sub> monolayer, as shown in Fig. 5, for comparison with the gas-adsorbed systems. We should note that in the BS distributions of the gas adsorbed systems, the spin-up is symmetric with the spin-down, revealing that gas adsorption has no impact on the magnetic property of the Ni-PtTe<sub>2</sub> monolayer.

For the BS of  $\text{O}_3$  and  $\text{NO}_2$  systems, one can see that the bandgaps are obtained as 0.021 and 0.281 eV, respectively, with different localizations for the top valence band and bottom

conduction band. That is,  $\text{O}_3$  and  $\text{NO}_2$  adsorptions largely deform the electronic property of the Ni-PtTe<sub>2</sub> monolayer, narrowing its bandgap significantly and altering its direct semiconducting property as well, which may be attributed to the induced novel states by the adsorption of  $\text{O}_3$  and  $\text{NO}_2$  that fall in the bandgap of the isolated Ni-PtTe<sub>2</sub> monolayer. Based on the dependence between the electrical resistance ( $\sigma$ ) and the bandgap as depicted in eqn (5),<sup>61</sup> wherein the  $\lambda$  is a constant,  $B_g$  is the bandgap,  $k$  is the Boltzmann constant and  $T$  is temperature, one can presume that the electrical resistance of the Ni-PtTe<sub>2</sub> monolayer could be largely reduced after adsorptions of such two gas species, especially for  $\text{O}_3$ . This provides the strong potential to explore the Ni-PtTe<sub>2</sub> monolayer as a gas sensor for the detection of  $\text{O}_3$  and  $\text{NO}_2$ .

$$\sigma = \lambda \times e^{(-B_g/2kT)} \quad (3)$$

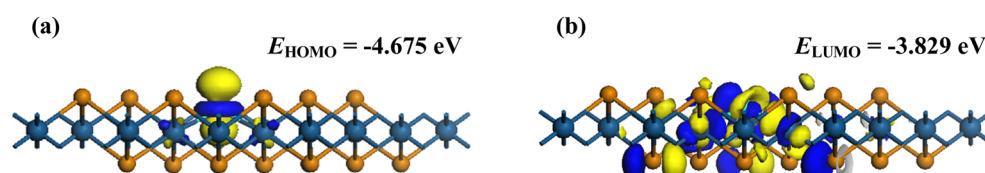


Fig. 5 HOMO (a) and LUMO (b) distributions of Ni-PtTe<sub>2</sub> monolayer.

Similar phenomena can also be found in the FMO distributions of the gas adsorbed systems, in comparison with the pure Ni–PtTe<sub>2</sub> counterpart. It is seen that the HOMO and LUMO are dominantly on the Ni dopant and their energies are –4.675 and –3.829 eV, respectively. At the same time, there are strong HOMO and LUMO distributions around Ni–O bonds in the O<sub>3</sub> system and around the Ni–N bond in the NO<sub>2</sub> system. These distributions of electron cloud manifest the strong interactions in the adsorptions and the strong binding force of Ni–O and Ni–N bonds.<sup>62</sup> For the O<sub>3</sub> system, the energies of HOMO and LUMO are obtained as –4.973 and –4.730 eV, respectively, while for the NO<sub>2</sub> system, those are obtained as –4.777 and –4.270 eV, respectively. Accordingly, the  $E_g$  is calculated to be 0.846 eV for the pure Ni–PtTe<sub>2</sub> monolayer, and 0.243 and 0.507 eV for O<sub>3</sub> and NO<sub>2</sub> systems, respectively. The results from the FMO analysis are in good accordance with those of the BS analysis in that the adsorptions of O<sub>3</sub> and NO<sub>2</sub> can remarkably narrow the bandgap (energy gap) of the Ni–PtTe<sub>2</sub> monolayer, therefore, reducing its electrical resistance significantly.

Moreover, from the orbital DOS of the bonding atoms, one can see that the Ni 3d orbital is highly overlapped with the O 2p orbital at –4.8 to –2.3, –1.6 to –0.1 and 0.5–1.0 eV, which reveals the strong orbital interaction in the Ni–O bond for O<sub>3</sub> adsorption, while the Ni 3d orbital is slightly hybrid with the N 2p orbital at –2.1, –0.5, and 0.2–0.5 eV, which revealed the much weaker binding force of the Ni–N bond in NO<sub>2</sub> adsorption compared with the Ni–O bond. These findings are consistent with the above analysis on the adsorption performance of Ni–PtTe<sub>2</sub> monolayer upon two gas species.

### 3.4 Gas sensor explorations

The above section indicated the change of bandgap based on BS analysis or of  $E_g$  based on FMO analysis for the Ni–PtTe<sub>2</sub> monolayer after adsorptions of two gases, therefore, the exploration of Ni–PtTe<sub>2</sub> monolayer as a resistance-type gas sensor is full of potential. As reported, the sensing response ( $S$ ) of a gas sensor can be evaluated by eqn (4):<sup>63</sup>

$$S = (\sigma_{\text{gas}}^{-1} - \sigma_{\text{pure}}^{-1})/\sigma_{\text{pure}}^{-1} \quad (4)$$

wherein the  $\sigma$  is electrical resistance that can be calculated by eqn (3).

Combined with eqn (3) and (4), the sensing responses of the Ni–PtTe<sub>2</sub> monolayer upon O<sub>3</sub> and NO<sub>2</sub> were obtained as –99.99% and –98.75%, according to the bandgap, and are to be –99.99% and –99.86%, respectively, according to the  $E_g$ . That is, the Ni–PtTe<sub>2</sub> monolayer has an admirable sensing response for O<sub>3</sub> and NO<sub>2</sub> detections, fully meeting the requirement for measurement by an electrochemical workstation<sup>64</sup> no matter what analyzing method is applied. Besides, the recovery property is further considered to analyze the possible reusability of the Ni–PtTe<sub>2</sub> monolayer for gas detection. Based on the van't Hoff–Arrhenius expression,<sup>65</sup> the recovery time ( $\tau$ ) for gas desorption from the Ni–PtTe<sub>2</sub> surface can be calculated by eqn (5):

$$\tau = A^{-1} e^{(-E_{\text{ad}}/K_B T)} \quad (5)$$

in which  $A$  is the attempt frequency (10<sup>12</sup> s<sup>–1</sup>),<sup>66</sup>  $T$  is temperature and  $K_B$  is Boltzmann constant (8.318 × 10<sup>–3</sup> kJ (mol K)<sup>–1</sup>). Therefore, the recovery time for the O<sub>3</sub> and NO<sub>2</sub> systems at room temperature (298 K) was calculated to be 1.54 × 10<sup>29</sup> and 4.42 × 10<sup>20</sup> s, and those even at 498 K were 4.43 × 10<sup>12</sup> and 3.43 × 10<sup>7</sup> s, respectively. In other words, the recycle detection for the Ni–PtTe<sub>2</sub> monolayer is almost impossible due to the extremely long recovery time for gas desorption from its surface. This also reflects the quite strong interactions in the O<sub>3</sub> and NO<sub>2</sub> system that gives rise to the large absolute value of  $E_{\text{ad}}$ . In this regard, ultraviolet light should be applied to illuminate the sensing material and facilitate the gas desorption from the nano-surface, which has been proven with desirable performance to significantly shut down the recovery time for the sensing material.<sup>67</sup>

Furthermore, we would like to mention that gas adsorptions on the Ni–PtTe<sub>2</sub> monolayer may largely change its work function (WF), which would bring about its sensing potential for O<sub>3</sub> and NO<sub>2</sub> detections based on the WF-measurement devices. For this purpose, we calculated the WF of the freestanding Ni–PtTe<sub>2</sub> monolayer and those after gas adsorptions, which are fully presented in Fig. 6. From this figure, one can see that the WF of the freestanding Ni–PtTe<sub>2</sub> monolayer is calculated to be 4.73 eV, which is somewhat larger than the WF of graphene (4.60 eV<sup>68</sup>), indicating the weaker electron affinity of the Ni–PtTe<sub>2</sub> monolayer. In other words, the Ni–PtTe<sub>2</sub> monolayer behaves relatively weaker electron-liberating properties than the graphene.<sup>69</sup> In addition, the WF in the O<sub>3</sub> and NO<sub>2</sub> systems are increased to 4.84 and 5.01 eV, respectively. That is, the WF of the Ni–PtTe<sub>2</sub> monolayer is increased by 2.32% after the adsorption of the O<sub>3</sub> molecule, and by 5.92% after the adsorption of the NO<sub>2</sub> molecule. These findings reveal that the WF of the Ni–PtTe<sub>2</sub> monolayer after adsorptions of two species is too small to be explored as a WF-based gas sensor for the detection of O<sub>3</sub> and NO<sub>2</sub> using the Kelvin oscillator device.<sup>70</sup>

In short, the Ni–PtTe<sub>2</sub> monolayer is a promising resistance-type gas sensing material to be explored for O<sub>3</sub> and NO<sub>2</sub> detections, by which the detection is based on the change of

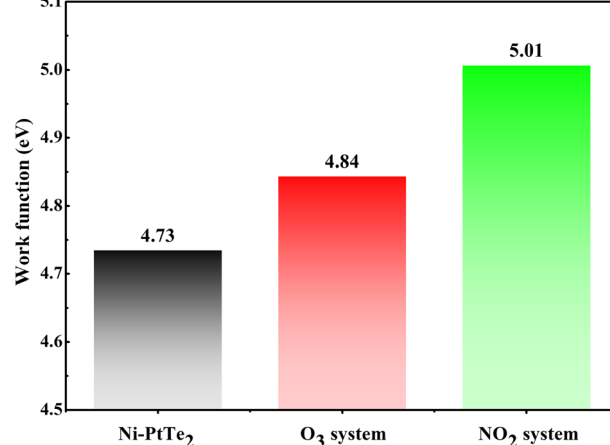


Fig. 6 WF of Ni–PtTe<sub>2</sub> system and Ni–PtTe<sub>2</sub>/gas systems.



electrical resistance. Therefore, from the aspect of operation status evaluation for the air-insulated switchgear, the Ni–PtTe<sub>2</sub> monolayer is a promising candidate *via* the detections of O<sub>3</sub> and NO<sub>2</sub>. However, such a sensor can only realize the one time operation for gas detection with a desirable sensing response, due to the long recovery time for recycling use.<sup>59</sup> Apart from that, the Ni–PtTe<sub>2</sub> monolayer is not suitable for the exploration of a WF-based O<sub>3</sub> and NO<sub>2</sub> gas sensor due to the limited WF change after their adsorptions.

## 4. Conclusions

In this work, we proposed the Ni–PtTe<sub>2</sub> monolayer as a novel and promising gas sensing material upon O<sub>3</sub> and NO<sub>2</sub> detection in the air-insulated switchgear, using the first-principles theory. The main conclusions are as follows:

(i) The  $E_{\text{form}}$  for Ni-doping on the PtTe<sub>2</sub> surface was calculated to be  $-0.55$  eV, which indicated the exothermicity and spontaneity for Te-substitution by a Ni atom.

(ii) Strong interactions, namely chemisorption, occurred in the O<sub>3</sub> and NO<sub>2</sub> systems given the significant  $E_{\text{ad}}$  values of  $-2.44$  and  $-1.93$  eV, respectively.

(iii) The sensing response of the Ni–PtTe<sub>2</sub> monolayer upon such two gas species is large enough to realize their detections, on the basis of the band structure and frontier molecular orbital analysis.

(iv) Ni–PtTe<sub>2</sub> monolayer is a promising resistance-type and one-shot gas sensor for O<sub>3</sub> and NO<sub>2</sub> detection with a strong sensing response, given the extremely long recovery time for gas desorption.

Overall, this work can broaden the family members of the gas sensing materials for the detection of the typical fault gases in the high-voltage insulation devices, which is significant to guarantee the good operation of the power system.

## Conflicts of interest

The authors declare no conflicts of interest.

## Acknowledgements

This work is supported by the National Natural Science Foundation of China (No. 52207175).

## References

- 1 T. Yoshida, H. Koga, T. Harada, S. Miki, M. Arioka, S. Sato, S. Yoshida, N. Inoue, A. Maruyama and T. Takeuchi, Insulation Technology in Dry Air and Vacuum for a 72 kV Low Pressured Dry Air Insulated Switchgear, *IEEE Trans. Power Energy*, 2008, **128**(1), 1439–1444.
- 2 W. Chen, Y. Gui, T. Li, H. Zeng, L. Xu and Z. Ding, Gas-sensing properties and mechanism of Pd-GaNNs for air decomposition products in ring main unit, *Appl. Surf. Sci.*, 2020, **531**, 147293.
- 3 P. Wagenaars, P. A. A. F. Wouters, P. C. J. M. van der Wielen and E. F. Steennis, Influence of Ring Main Units and Substations on Online Partial-Discharge Detection and Location in Medium-Voltage Cable Networks, *IEEE Trans. Power Delivery*, 2011, **26**(2), 1064–1071.
- 4 D.-Y. Lim and S. Bae, Study on oxygen/nitrogen gas mixtures for the surface insulation performance in gas insulated switchgear, *IEEE Trans. Dielectr. Electr. Insul.*, 2015, **22**(3), 1567–1576.
- 5 H. Cui, T. Liu, Y. Zhang, Ru-InN Monolayer as a Gas Scavenger to Guard the Operation Status of SF6 Insulation Devices: A First-Principles Theory, *IEEE Sens. J.*, 2019, **19**(13), 5249–5255.
- 6 H. Cui, Y. Guo, Z. Qi and G. Zhang, Pd-doped PtSe<sub>2</sub> monolayer with strain-modulated effect for sensing SF6 decomposed species: a first-principles study, *J. Mater. Res. Technol.*, 2022, **18**, 629–636.
- 7 H. Cui, Q. Zhang, H. Liu and X. Peng, Janus PtSSe monolayer: a novel strain-modulated buddy for SOF2 sensing, *Vacuum*, 2022, **198**, 110887.
- 8 J. Chu, Q. Wang, A. Yang, J. Pan, Y. Liu, H. Yuan, M. Rong and X. Wang, Method of sieving the optimal NO<sub>2</sub> sensitive material, *Sens. Actuators, B*, 2023, **375**, 132929.
- 9 H. Wu, Y. Xia, C. Zhang, S. Xie, S. Wu and H. Cui, Adsorptions of C5F10O decomposed compounds on the Cu-decorated NiS<sub>2</sub> monolayer: a first-principles theory, *Mol. Phys.*, 2023, e2163715.
- 10 J. Chu, Q. Wang, Y. Liu, J. Pan, H. Yuan, A. Yang, X. Wang and M. Rong, Fault Diagnosis of SF6-insulated Equipment by Micro Gas Sensor Array, *IEEE Trans. Power Deliv.*, 2022, 222–230.
- 11 S. Muhammad, E. Montes, N. Singh and U. Schwingenschlögl, Superior Gas Sensing Properties of Monolayer PtSe<sub>2</sub>, *Adv. Mater. Interfaces*, 2017, **4**(5), 1600911.
- 12 H. Yang, Z. Wang, H. Ye, K. Zhang, X. Chen and G. Zhang, Promoting sensitivity and selectivity of HCHO sensor based on strained InP<sub>3</sub> monolayer: a DFT study, *Appl. Surf. Sci.*, 2018, **459**, 554–561.
- 13 H. Cui, X. Zhang, J. Zhang and Y. Zhang, Nanomaterials-based gas sensors of SF6 decomposed species for evaluating the operation status of high-voltage insulation devices, *High Voltage*, 2019, **4**(4), 242–258.
- 14 R. Srivastava, H. Suman, S. Shrivastava and A. Srivastava, DFT analysis of pristine and functionalized zigzag CNT: a case of H<sub>2</sub>S sensing, *Chem. Phys. Lett.*, 2019, **731**, 136575.
- 15 H. Cui, D. Chen, Y. Zhang and X. Zhang, Dissolved gas analysis in transformer oil using Pd catalyst decorated MoSe<sub>2</sub> monolayer: A first-principles theory, *Sustain. Mater. Technol.*, 2019, **20**, e00094.
- 16 X. Zhang, Y. Lei, X. Wu and W. Hu, Experimental Sensing and Density Functional Theory Study of H<sub>2</sub>S and SOF2 Adsorption on Au-Modified Graphene, *Adv. Sci.*, 2015, **2**(11), 612.
- 17 X. Zhang, L. Yu, Y. Gui and W. Hu, First-principles study of SF6 decomposed gas adsorbed on Au-decorated graphene, *Appl. Surf. Sci.*, 2016, **367**, 259–269.
- 18 M. Yar, M. A. Hashmi and K. Ayub, Nitrogenated holey graphene (C<sub>2</sub>N) surface as highly selective electrochemical sensor for ammonia, *J. Mol. Liq.*, 2019, **296**, 111929.



19 G. X. Chen, H. F. Li, D. D. Wang, S. Q. Li, X. B. Fan and J. M. Zhang, Adsorption of toxic gas molecules on pristine and transition metal doped hexagonal GaN monolayer: a first-principles study, *Vacuum*, 2019, **165**, 35–45.

20 M. Chhowalla, H. S. Shin, G. Eda, L. J. Li, K. P. Loh and H. Zhang, The chemistry of two-dimensional layered transition metal dichalcogenide nanosheets, *Nat. Chem.*, 2013, **5**(4), 263–275.

21 A. Shokri and N. Salami, Gas sensor based on MoS<sub>2</sub> monolayer, *Sens. Actuators, B*, 2016, **236**, 378–385.

22 Y. F. Lin, Y. Xu, S. T. Wang, S. L. Li, M. Yamamoto, A. Aparecido-Ferreira, W. Li, H. Sun, S. Nakaharai and W. B. Jian, Ambipolar MoTe<sub>2</sub> Transistors and Their Applications in Logic Circuits, *Adv. Mater.*, 2014, **26**(20), 3263–3269.

23 H. Cui, X. Zhang, G. Zhang and J. Tang, Pd-doped MoS<sub>2</sub> monolayer: a promising candidate for DGA in transformer oil based on DFT method, *Appl. Surf. Sci.*, 2019, **470**, 1035–1042.

24 P. Manchanda, A. Enders, D. J. Sellmyer and R. Skomski, Hydrogen-induced ferromagnetism in two-dimensional Pt dichalcogenides, *Phys. Rev. B*, 2016, **94**(10), 104426.

25 D. Wu, C. Jia, F. Shi, L. Zeng, P. Lin, L. Dong, Z. Shi, Y. Tian, X. Li and J. Jie, Mixed-dimensional PdSe<sub>2</sub>/SiNWA heterostructure based photovoltaic detectors for self-driven, broadband photodetection, infrared imaging and humidity sensing, *J. Mater. Chem. A*, 2020, **8**(7), 3632–3642.

26 D. Li, X. Rao, L. Zhang, Y. Zhang, S. Ma, L. Chen and Z. Yu, First-Principle Insight into the Ru-Doped PtSe<sub>2</sub> Monolayer for Detection of H<sub>2</sub> and C<sub>2</sub>H<sub>2</sub> in Transformer Oil, *ACS Omega*, 2020, **5**(49), 31872–31879.

27 Y. Wang, L. Li, W. Yao, S. Song, J. T. Sun, J. Pan, X. Ren, C. Li, E. Okunishi, Y.-Q. Wang, E. Wang, Y. Shao, Y. Y. Zhang, H.-t. Yang, E. F. Schwier, H. Iwasawa, K. Shimada, M. Taniguchi, Z. Cheng, S. Zhou, S. Du, S. J. Pennycook, S. T. Pantelides and H.-J. Gao, Monolayer PtSe<sub>2</sub>, a New Semiconducting Transition-Metal-Dichalcogenide, Epitaxially Grown by Direct Selenization of Pt, *Nano Lett.*, 2015, **15**(6), 4013–4018.

28 H. Cui, P. Jia and X. Peng, Adsorption of SO<sub>2</sub> and NO<sub>2</sub> molecule on intrinsic and Pd-doped HfSe<sub>2</sub> monolayer: a first-principles study, *Appl. Surf. Sci.*, 2020, **513**, 145863.

29 H. Cui, Z. Feng, W. Wang, X. Peng and J. Hu, Adsorption Behavior of Pd-Doped PtS<sub>2</sub> Monolayer Upon SF<sub>6</sub> Decomposed Species and the Effect of Applied Electric Field, *IEEE Sens. J.*, 2022, **22**(7), 6764–6771.

30 J.-H. Ren, Z.-H. Yang, T. Huang, W.-Q. Huang, W.-Y. Hu and G.-F. Huang, Monolayer PtTe<sub>2</sub>: a promising candidate for NO<sub>2</sub> sensor with ultrahigh sensitivity and selectivity, *Phys. E*, 2021, **134**, 114925.

31 Q. Wan, X. Chen and S. Xiao, Ru-Doped PtTe<sub>2</sub> Monolayer as a Promising Exhaled Breath Sensor for Early Diagnosis of Lung Cancer: A First-Principles Study, *Chemosensors*, 2022, **10**(10), 428.

32 J. Du, P. Song, L. Fang, T. Wang, Z. Wei, J. Li and C. Xia, Elastic, electronic and optical properties of the two-dimensional PtX<sub>2</sub> (X= S, Se, and Te) monolayer, *Appl. Surf. Sci.*, 2018, **435**, 476–482.

33 Y. Shan, T. Li and L. Liu, Dopant-induced magnetism in platinum telluride monolayer regulated by strain engineering, *Phys. E*, 2020, **116**, 113741.

34 M. Wang, T.-J. Ko, M. S. Shawkat, S. S. Han, E. Okogbue, H.-S. Chung, T.-S. Bae, S. Sattar, J. Gil and C. Noh, Wafer-scale growth of 2D PtTe<sub>2</sub> with layer orientation tunable high electrical conductivity and superior hydrophobicity, *ACS Appl. Mater. Interfaces*, 2020, **12**(9), 10839–10851.

35 W. Chen, J.-m. Zhang, X.-g. Wang, Q.-l. Xia, Y.-z. Nie and G.-h. Guo, Ferromagnetism in PtTe<sub>2</sub> monolayer introduced by doping 3d transition metal atoms and group VA and VIIB atoms, *J. Magn. Magn. Mater.*, 2021, **518**, 167433.

36 H. Cui, X. Zhang, Y. Li, D. Chen and Y. Zhang, First-principles insight into Ni-doped InN monolayer as a noxious gases scavenger, *Appl. Surf. Sci.*, 2019, **494**, 859–866.

37 X. Zhou, W. Chu, Y. Zhou, W. Sun and Y. Xue, DFT simulation on H<sub>2</sub> adsorption over Ni-decorated defective h-BN nanosheets, *Appl. Surf. Sci.*, 2018, **439**, 246–253.

38 H. Cui, C. Yan, P. Jia and W. Cao, Adsorption and sensing behaviors of SF<sub>6</sub> decomposed species on Ni-doped C<sub>3</sub>N monolayer: a first-principles study, *Appl. Surf. Sci.*, 2020, **512**, 145759.

39 D. Zhang, Z. Yang, P. Li, M. Pang and Q. Xue, Flexible self-powered high-performance ammonia sensor based on Au-decorated MoSe<sub>2</sub> nanoflowers driven by single layer MoS<sub>2</sub>-flake piezoelectric nanogenerator, *Nano Energy*, 2019, **65**, 103974.

40 P. Li, Q. Hong, T. Wu and H. Cui, SOF<sub>2</sub> sensing by Rh-doped PtS<sub>2</sub> monolayer for early diagnosis of partial discharge in the SF<sub>6</sub> insulation device, *Mol. Phys.*, 2021, **119**(11), e1919774.

41 G. Liu, Y. Gan, R. Quhe and P. Lu, Strain dependent electronic and optical properties of PtS<sub>2</sub> monolayer, *Chem. Phys. Lett.*, 2018, **709**, 65–70.

42 A. Tkatchenko, R. A. Di Stasio Jr, M. Head-Gordon and M. Scheffler, Dispersion-corrected Møller-Plesset second-order perturbation theory, *J. Chem. Phys.*, 2009, **131**(9), 171.

43 D. Chen, X. Zhang, J. Tang, H. Cui and Y. Li, Noble metal (Pt or Au)-doped monolayer MoS<sub>2</sub> as a promising adsorbent and gas-sensing material to SO<sub>2</sub>, SOF<sub>2</sub> and SO<sub>2</sub>F<sub>2</sub>: a DFT study, *Appl. Phys. A: Mater. Sci. Process.*, 2018, **124**(2), 194.

44 Y. Ji, Y. Liu, Y. Xu, L. Liu and Y. Chen, Electronic and optical properties of sulfur vacancy-defect monolayer PtS<sub>2</sub>: a first-principles study, *Mater. Chem. Phys.*, 2020, 123588–123595.

45 D. Zhang, Q. Li, P. Li, M. Pang and Y. Luo, Fabrication of Pd-decorated MoSe<sub>2</sub> nanoflowers and density functional theory simulation toward ammonia sensing, *IEEE Electron Device Lett.*, 2019, **40**(4), 616–619.

46 L. Kou, T. Frauenheim and C. Chen, Phosphorene as a Superior Gas Sensor: Selective Adsorption and Distinct I–V Response, *J. Phys. Chem. Lett.*, 2014, **5**(15), 2675–2681.

47 L. Xu, Y. Gui, W. Li, Q. Li and X. Chen, Gas-sensing properties of Ptn-doped WSe<sub>2</sub> to SF<sub>6</sub> decomposition products, *J. Ind. Eng. Chem.*, 2021, **97**, 452–459.



48 P. Pykkö and M. Atsumi, Molecular single-bond covalent radii for elements 1-118, *Chemistry*, 2009, **15**(1), 186–197.

49 Z. M. Ao, J. Yang, S. Li and Q. Jiang, Enhancement of CO detection in Al doped graphene, *Chem. Phys. Lett.*, 2008, **461**(4), 276–279.

50 B. Jing, Z. Ao, Z. Teng, C. Wang, J. Yi and T. An, Density functional theory study on the effects of oxygen groups on band gap tuning of graphitic carbon nitrides for possible photocatalytic applications, *Sustain. Mater. Technol.*, 2018, **16**, 12–22.

51 L. R. Murphy, T. L. Meek, A. L. Allred and L. C. Allen, Evaluation and test of Pauling's electronegativity scale, *J. Phys. Chem. A*, 2000, **104**(24), 5867–5871.

52 X.-Y. Liang, N. Ding, S.-P. Ng and C.-M. L. Wu, Adsorption of gas molecules on Ga-doped graphene and effect of applied electric field: a DFT study, *Appl. Surf. Sci.*, 2017, **411**, 11–17.

53 S. Zhai, X. Jiang, D. Wu, L. Chen, Y. Su, H. Cui and F. Wu, Single Rh atom decorated pristine and S-defected PdS<sub>2</sub> monolayer for sensing thermal runaway gases in a lithium-ion battery: a first-principles study, *Surf. Interfaces*, 2023, **37**, 102735.

54 J. Huang, J. Chu, Z. Wang, J. Zhang, A. Yang, X. Li, C. Gao, H. Huang, X. Wang, Y. Cheng and M. Rong, Chemisorption of NO<sub>2</sub> to MoS<sub>2</sub> Nanostructures and its Effects for MoS<sub>2</sub> Sensors, *ChemNanoMat*, 2019, **5**(9), 1123–1130.

55 Y. Wang, X. Yang, C. Hu and T. Wu, Rh-Doped ZnO Monolayer as a Potential Gas Sensor for Air Decomposed Species in a Ring Main Unit: A First-Principles Study, *ACS Omega*, 2021, **6**(24), 15878–15884.

56 A. S. Rad and D. Zareyee, Adsorption properties of SO<sub>2</sub> and O<sub>3</sub> molecules on Pt-decorated graphene: a theoretical study, *Vacuum*, 2016, **130**, 113–118.

57 S. W. Han, G. B. Cha, Y. Park and S. C. Hong, Hydrogen physisorption based on the dissociative hydrogen chemisorption at the sulphur vacancy of MoS<sub>2</sub> surface, *Sci. Rep.*, 2017, **7**(1), 7152–7159.

58 C. Hu, Q. Shi, X. Yang, T. Wu and Z. Pu, Adsorption and sensing characteristics of air decomposed species onto pyridine-like PdN<sub>3</sub>-doped CNT: a first-principles study, *Carbon Lett.*, 2022, **32**(1), 109–117.

59 H. Cui, G. Zhang, X. Zhang and J. Tang, Rh-doped MoSe<sub>2</sub> as toxic gas scavenger: a first-principles study, *Nanoscale Adv.*, 2019, **2019**(1), 772–780.

60 D. H. Keum, S. Cho, J. H. Kim, D. H. Choe, H. J. Sung, M. Kan, H. Kang, J. Y. Hwang, S. W. Kim and H. Yang, Bandgap opening in few-layered monoclinic MoTe<sub>2</sub>, *Nat. Phys.*, 2015, **11**(6), 482–486.

61 H. Wei, Y. Gui, J. Kang, W. Wang and C. Tang, A DFT Study on the Adsorption of H<sub>2</sub>S and SO<sub>2</sub> on Ni Doped MoS<sub>2</sub> Monolayer, *Nanomaterials*, 2018, **8**(9), 646.

62 X. Zhang, J. Wang, D. Chen and L. Liu, The adsorption performance of harmful gas on Cu doped WS<sub>2</sub>: a First-principle study, *Mater. Today Commun.*, 2021, 102488.

63 S. Li, *Semiconductor physical electronics*, Springer Science & Business Media, 2012.

64 D. Zhang, Z. Wu, X. Zong and Y. Zhang, Fabrication of polypyrrole/Zn<sub>2</sub>SnO<sub>4</sub> nanofilm for ultra-highly sensitive ammonia sensing application, *Sens. Actuators, B*, 2018, **274**, 575–586.

65 Y. H. Zhang, Y. B. Chen, K. G. Zhou, C. H. Liu, J. Zeng, H. L. Zhang and Y. Peng, Improving gas sensing properties of graphene by introducing dopants and defects: a first-principles study, *Nanotechnology*, 2009, **20**(18), 185504.

66 S. Peng, K. Cho, P. Qi and H. Dai, Ab initio study of CNT NO<sub>2</sub> gas sensor, *Chem. Phys. Lett.*, 2004, **387**(4), 271–276.

67 E. Wu, Y. Xie, B. Yuan, H. Zhang, X. Hu, J. Liu and D. Zhang, Ultra-sensitive and Fully Reversible NO<sub>2</sub> Gas Sensing based on p-type MoTe<sub>2</sub> Under ultra-violet Illumination, *ACS Sens.*, 2018, **3**(9), 1719–1726.

68 Y. J. Yu, Y. Zhao, S. Ryu, L. E. Brus, K. S. Kim and P. Kim, Tuning the graphene work function by electric field effect, *Nano Lett.*, 2009, **9**(10), 3430–3434.

69 Z. Jiang, Q. Pan, M. Li, T. Yan and T. Fang, Density functional theory study on direct catalytic decomposition of ammonia on Pd (111) surface, *Appl. Surf. Sci.*, 2014, **292**, 494–499.

70 N. B. Tanvir, O. Yurchenko, E. Laubender and G. Urban, Investigation of low temperature effects on work function based CO<sub>2</sub> gas sensing of nanoparticulate CuO films, *Sens. Actuators, B*, 2017, **247**, 968–974.

